Ultrahigh-power micrometre-sized supercapacitors based on onion-like carbon

David Pech[1,2], Magali Brunet[1,2]*, Hugo Durou[1,2], Peihua Huang[1,2,4], Vadym Mochalin[3], Yury Gogotsi[3], Pierre-Louis Taberna[4] and Patrice Simon[4]

Electrochemical capacitors, also called supercapacitors, store energy in two closely spaced layers with opposing charges, and are used to power hybrid electric vehicles, portable electronic equipment and other devices[1]. By offering fast charging and discharging rates, and the ability to sustain millions of cycles[2-5], electrochemical capacitors bridge the gap between batteries, which offer high energy densities but are slow, and conventional electrolytic capacitors, which are fast but have low energy densities. Here, we demonstrate microsupercapacitors with powers per volume that are comparable to electrolytic capacitors, capacitances that are four orders of magnitude higher, and energies per volume that are an order of magnitude higher. We also measured discharge rates of up to 200 V s^{-1}, which is three orders of magnitude higher than conventional supercapacitors. The microsupercapacitors are produced by the electrophoretic deposition of a several-micrometre-thick layer of nanostructured carbon onions[6,7] with diameters of 6–7 nm. Integration of these nanoparticles in a microdevice with a high surface-to-volume ratio, without the use of organic binders and polymer separators, improves performance because of the ease with which ions can access the active material. Increasing the energy density and discharge rates of supercapacitors will enable them to compete with batteries and conventional electrolytic capacitors in a number of applications.

The recent boom in multifunction portable electronic equipment and the increasing need for wireless sensor networks for the development of smart environments has raised the problem of developing sufficiently compact and/or flexible energy storage. Designing efficient, miniaturized energy-storage devices that can achieve high energy delivery or harvesting at high discharge rates with a lifetime that matches or exceeds that of the machine being powered remains a challenge[8]. Integrating the storage element as close as possible to the electronic circuit (directly on a chip) is another challenge. Because electrochemical energy storage in batteries occurs by means of volumetric reactions[9], the charge discharge rate and specific power of the best batteries (lithium-ion) are limited by the rate of solid-state diffusion. Also, the redox reactions and expansion–contraction of the active material limit battery lifetime to just hundreds or thousands of cycles. These problems can only be partially resolved by using nanostructured materials[10,11]. The properties of thin-film batteries, despite their excellent energy per unit volume, drop dramatically in the microscale range[12].

Electrochemical capacitors (ECs) store energy using an accumulation of ions of opposite charge in a double layer at electrochemically stable, high specific surface area electrodes. The high surface-to-volume ratio of the active material leads to the high

energy and power densities of ECs; this is further enhanced in microsupercapacitors[13,14]. Porous activated, templated[15] and carbide-derived carbons[16], multi- and single-walled carbon nanotubes[17] and multilayer graphene[18] have been used as the electrode materials in supercapacitors. However, very few studies have been performed using spherical carbon nanoparticles[19–21], which do not have the narrow pores that in activated carbons or nanotubes may cause the transport of ions to be the rate-controlling factor limiting the charge/discharge rate. This Letter reports the electrochemical performance of onion-like carbon (OLC) electrodes assembled in a microsized device, which was able to cycle at a scan rate of 200 V s^{-1}.

OLCs are quasi-spherical nanoparticles consisting of concentric graphitic shells[22]. Although there are many methods by which OLCs may be produced, the annealing of detonation nanodiamond powders (Supplementary Fig. S1a–d) is inexpensive and the only widely used method that allows the synthesis of large amounts of OLC[23]. In an ideal case, they could be considered as multishell giant fullerenes, but real particles have discontinuous and defective shells when synthesized at temperatures below 1,800 °C (as shown in Supplementary Fig. S1d) or polygonized shells when higher temperatures or longer times are used.

Carbon onions offer a moderate specific surface area ($\sim$500 m^2 g^{-1}; Supplementary Table S1) compared to that of activated carbons, but this surface is fully accessible to ion adsorption (Fig. 1a) because there is no porous network inside the particles. Accordingly, OLCs have demonstrated modest gravimetric capacitance in previous studies, at about one-third that of activated carbons[24]. Based on these results, we anticipated that the accessible external surface area of the carbon onions would be appealing in the design of thin electrodes for microsystems, where the limited volume available for device integration onto chips drives the technology.

OLC particles were produced by annealing nanodiamond powder at 1,800 °C (Fig. 1b) then deposited from colloidal suspensions using an electrophoretic deposition technique (EPD) onto interdigital gold current collectors patterned on silicon wafers. This method allows electrodes to be prepared without the use of an organic binder (Fig. 1c; see also Supplementary Table S2). An adherent layer of OLC was obtained on the gold current collectors, with a well-defined pattern and no short circuit between the electrodes (Fig. 1d). The microdevice was constructed with 16 interdigital electrodes with thicknesses of 7 μm (eight electrodes per polarity), as shown in Fig. 1e.

Cyclic voltammograms (CVs) were recorded at scan rates from 1 to 200 V s^{-1} to test the power capability of the microsystem. A reproducible and stable capacitive behaviour (up to 10,000

[1]CNRS, LAAS, 7 avenue du Colonel Roche, F-31077 Toulouse, France, [2]Université de Toulouse, UPS, INSA, INP, ISAE, LAAS, F-31077 Toulouse, France, [3]Department of Materials Science Engineering and A.J. Drexel Nanotechnology Institute, Drexel University, Philadelphia, Pennsylvania 19104, USA, [4]Université Paul Sabatier de Toulouse, CIRIMAT, UMR CNRS 5085, 118 route de Narbonne, F-31062 Toulouse, France. *e-mail: mbrunet@laas.fr
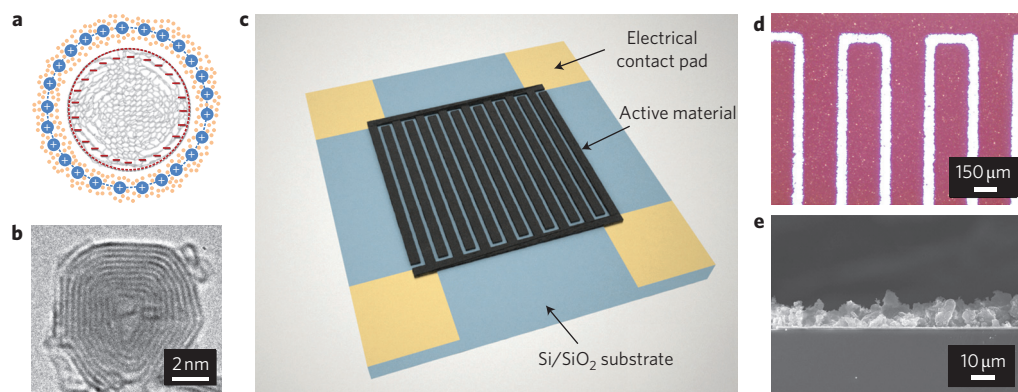
Figure 1 | Design of the interdigital microsupercapacitor with OLC electrodes. a, Cross-section of a charged zero-dimensional OLC (grey) capacitor, consisting of two layers of charges (blue and pink) forming the inner and outer spheres, respectively. **b**, Transmission electron microscopy image of a carbon onion produced at 1,800 °C. Lattice spacing between the bent graphitic layers in the onions is close to 0.35 nm. **c**, Schematic of the microdevice (25 mm²). Two gold current collectors made of 16 interdigital fingers were deposited by evaporation on an oxidized silicon substrate and patterned using a conventional photolithography/etching process. Carbon onions (active material) were then deposited by electrophoretic deposition onto the gold current collectors. **d**, Optical image of the interdigital fingers with 100-μm spacing. **e**, Scanning electron microscope image of the cross-section of the carbon onion electrode. A volumetric power density of 1 kW cm^{-3} was obtained with a deposited layer thickness in the micrometre range, not the nanometre range.
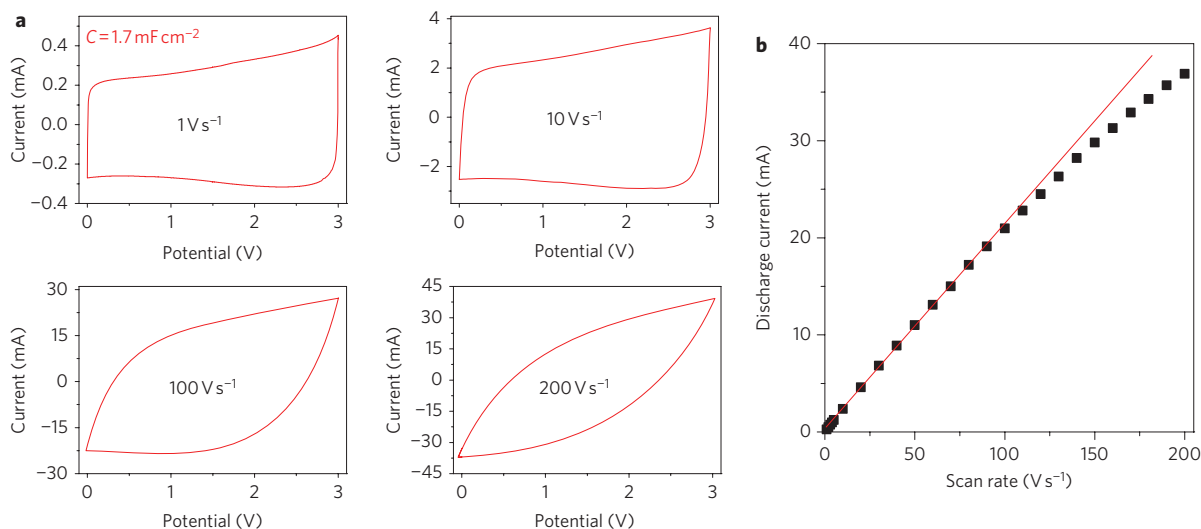
Figure 2 | Electrochemical characterizations of the microdevices. a, CVs obtained at different scan rates in a 1 M Et$_4$NBF$_4$/anhydrous propylene carbonate on a 16-interdigital electrochemical microcapacitor with a 7-μm-thick OLC deposit. A typical rectangular shape, as expected for double-layer capacitive materials, is observed at an ultrahigh scan rate over a 3 V potential window. **b**, Evolution of the discharge current versus scan rate. A linear dependence is obtained up to at least 100 V s^{-1} in the capacitive region, indicating an ultrahigh power ability for the microdevices.

cycles; Supplementary Fig. S2) was obtained for the microdevice over a 3 V potential window in a 1 M solution of tetraethylammonium tetrafluoroborate in propylene carbonate, with a linear dependence of the discharge current on the scan rate and low resistive contributions up to 100 V s^{-1} (Fig. 2). This scan rate is more than two orders of magnitude higher than any result reported with alternative devices[15,25], including microdevices[13,14] and microcavity electrodes[26–28]. Furthermore, the more interdigital electrodes per unit area, the more power is extracted from the microdevice. This is explained by a significant reduction in the mean ionic diffusion path between the two electrodes (Supplementary Fig. S3 and Table S2).

The specific capacitance of this microdevice was 0.9 mF cm^{-2} at 100 V s^{-1}, which is comparable to values reported in the literature at much lower scan rates (1–100 mV s^{-1}) for electrochemical double-layer microcapacitors (0.4–2 mF cm^{-2})[13,14,29]. The high scan rate, representative of a high instantaneous power, is thus concomitant with a high specific capacitance, which is explained by the

significant (7 μm) thickness of the active film (Fig. 1). The combination of carbon onions with a fully accessible surface area, with a binder-free deposition technique and a micro-interdigital device design led to this high power/energy performance.

To highlight the effect of the endohedral structure of carbon onions on cell performance, a 5.0-μm-thick high-surface-area activated carbon (AC) (1,700–1,800 m² g^{-1}, Kuraray Chemical Co.) was used as the active material in a microdevice made of 16 interdigital electrodes. The deposition technique and the cell assembly were kept the same. Figure 3a,b shows a comparison of the stack capacitance and energy of microdevices with AC and OLC. Despite a higher capacitance (9.0 F cm^{-3}, compared to 1.3 F cm^{-3} for OLC) and a capacitive behaviour up to 1 V s^{-1} (Supplementary Fig. S4), the capacitance of microdevices with AC fell quickly at a higher scan rate, indicating a severe decrease in the instantaneous power of AC- relative to OLC-based microdevices because of the limitation of ion transfer in the inner porous network of the AC. Both microdevices exhibited a low equivalent series resistance (ESR;
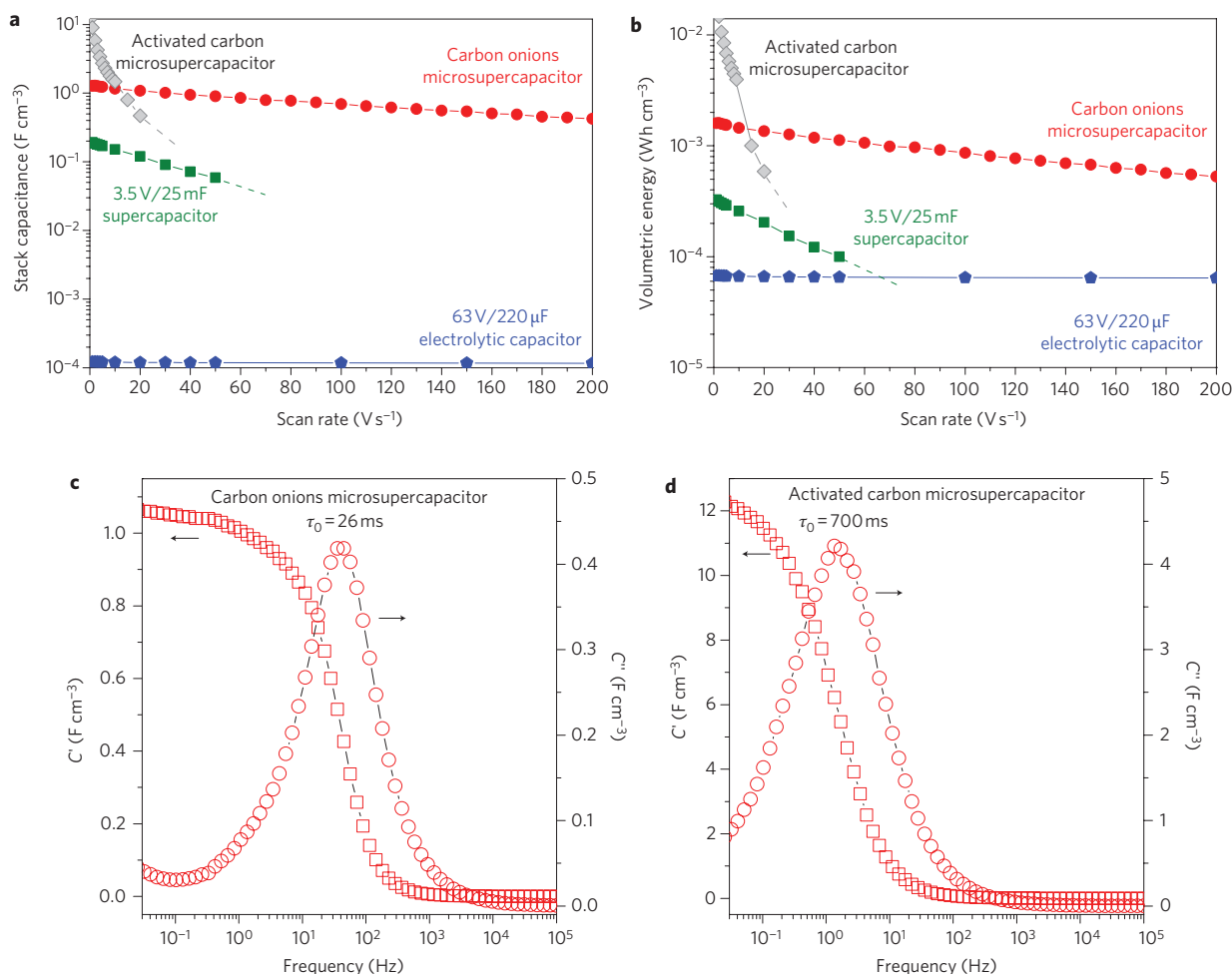
Figure 3 | Comparison of microsupercapacitors and other energy storage devices. a, Evolution of the stack capacitance versus scan rate. Carbon onion microsupercapacitors can sustain very high scan rates, like electrolytic capacitors. The stack capacitance is, however, four orders of magnitude higher than that of the electrolytic capacitors. **b**, Evolution of the volumetric energy of different energy-storage devices. **c,d**, Evolution of the real and imaginary part (C' and C'') of the stack capacitance of a 16-interdigital electrochemical microcapacitor based on OLC (**c**) and AC (**d**). An extremely low relaxation time constant τ_0 (26 ms) was obtained for the OLC, revealing fast accessibility of the ions for electrosorption.
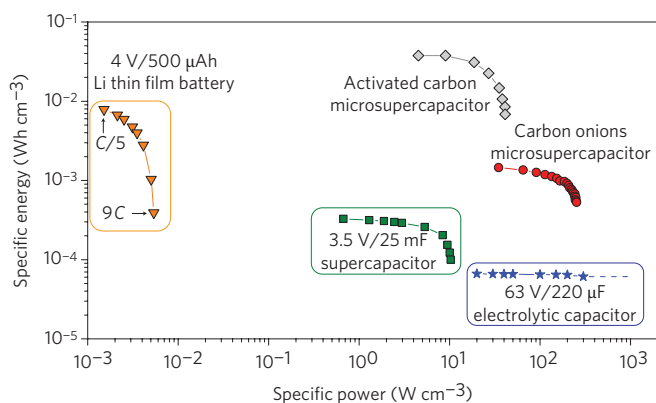
Figure 4 | Comparison, in a Ragone plot, of the specific energy and power density (per cm³ of stack) of typical electrolytic capacitors, supercapacitors and batteries with the microdevices. All the devices (macro and micro) were tested under the same dynamic conditions. A very high energy density was obtained with the AC-based microsupercapacitor, whereas ultrahigh power density was obtained with the OLC-based microsupercapacitor.

Supplementary Fig. S5), but because the entire outer surface of the OLC is fully accessible to ion adsorption/desorption, it is characterized by an extremely small characteristic relaxation time constant τ_0 of 26 ms (τ_0 being the minimum time needed to discharge all the energy from the device with an efficiency of greater than 50% (ref. 30); Fig. 3c), which is much lower than that of the AC-based microdevice ($\tau_0 = 700$ ms; Fig. 3d) or OLC-based macroscopic devices ($\tau_0 > 1$ s)[24]. It has been shown theoretically that the positive curvature causes the normalized capacitance to increase with decreasing particle size[31]. Therefore, OLC has the potential for delivering high power and energy as one of the smallest endohedral particles available.

A comparison of the different energy storage devices designed for power microelectronics applications (a 500-μAh thin-film lithium battery, a 25-mF supercapacitor and an electrolytic capacitor of the same absolute capacitance), tested under the same dynamic conditions, is presented in the Ragone plot of Fig. 4. This shows the relationship between the volumetric energy density and power density of the stack (comprising the current collectors, the active material and the separator) for the energy storage devices tested. The specific power and specific energy were calculated by integrating the CVs at different rates (see Supplementary Information for

details). The electrolytic capacitors were able to perform at a very high scan rate, but had a stack capacitance that was four orders of magnitude lower than the microdevices, and a specific energy that was more than one order of magnitude lower. Meanwhile, the lithium battery and conventional supercapacitors could not provide the ultrafast discharge rate demonstrated by the microdevices. Electrochemical microcapacitors with ACs demonstrate an energy density of 1×10^{-2} Wh cm^{-3} (10 Wh l^{-1} using conventional units). With OLC, a maximum power density is obtained that is 100 times higher, at close to 1 kW cm^{-3} (1 MW l^{-1}). These therefore represent a new generation of devices, approaching the power of electrolytic capacitors, but having orders of magnitude larger energy density. To the best of our knowledge, there are no other devices available, including state-of-the-art microcapacitors[32] that show the same performance characteristics.

This finding addresses the need for microscale energy storage in numerous areas where electrolytic capacitors cannot provide sufficient volumetric energy density, such as nomad electronics, wireless sensor networks, biomedical implants, active radiofrequency identification (RFID) tags and embedded microsensors. These applications can be extended to larger devices by scaling up the electrode surface and using high-resolution ink-jet, transfer printing and other high-throughput techniques that are suitable for mass production. Further improvements in the configuration of the patterned electrodes (for example, decreasing the space between the electrodes down to the nanoscale), in the material properties (for example, decreasing the onion size), the density and homogeneity of the deposited electrode, and viscosity/conductivity of electrolytes are expected to allow the design of high-energy supercapacitors with even higher power and energy characteristics.

References

1. Miller, J. R. & Simon, P. Electrochemical capacitors for energy management. *Science* **321,** 651–652 (2008).
2. Conway, B. E. *Electrochemical Supercapacitors: Scientific Fundamentals and Technological Applications* (Kluwer, 1999).
3. Kötz, R. & Carlen, M. Principles and applications of electrochemical capacitors. *Electrochim. Acta* **45,** 2483–2498 (2000).
4. Burke, A. R&D considerations for the performance and application of electrochemical capacitors. *Electrochim. Acta* **53,** 1083–1091 (2007).
5. Simon, P. & Gogotsi, Y. Materials for electrochemical capacitors. *Nature Mater.* **7,** 845–854 (2008).
6. Sano, N., Wang, H., Chhowalla, M., Alexandrou, I. & Amaratunga, G. A. J. Nanotechnology: synthesis of carbon 'onions' in water. *Nature* **414,** 506–507 (2001).
7. Gogotsi, Y. (ed.) *Carbon Nanomaterials* (CRC, 2006).
8. Chmiola, J., Largeot, C., Taberna, P.-L., Simon, P. & Gogotsi, Y. Monolithic carbide-derived carbon films for micro-supercapacitors. *Science* **328,** 480–483 (2010).
9. Tarascon, J.-M. & Armand, M. Issues and challenges facing rechargeable lithium batteries. *Nature* **414,** 359–367 (2001).
10. Aricò, A. S., Bruce, P., Scrosati, B., Tarason, J.-M. & Van Schalkwijk, W. Nanostructured materials for advanced energy conversion and storage devices. *Nature Mater.* **4,** 366–377 (2005).
11. Woo Lee, S. *et al.* High-power lithium batteries from functionalized carbon-nanotube electrodes. *Nature Nanotech.* **5,** 531–537 (2010).
12. Long, J. W., Dunn, B., Rolison, D. R. & White, H. S. Three-dimensional battery architectures. *Chem. Rev.* **104,** 4463–4492 (2004).
13. In, H. J., Kumar, S., Shao-Horn, Y. & Barbastathis, G. Origami fabrication of nanostructured, three-dimensional devices: electrochemical capacitors with carbon electrodes. *Appl. Phys. Lett.* **88,** 0831041 (2006).
14. Pech, D. *et al.* Elaboration of a microstructured inkjet-printed carbon electrochemical capacitor. *J. Power Sources* **195,** 1266–1269 (2010).
15. Kajdos, A., Kvit, A., Jones, F., Jagiello, J. & Yushin, G. Tailoring the pore alignment for rapid ion transport in microporous carbons. *J. Am. Chem. Soc.* **132,** 3252–3253 (2010).
16. Dash, R. *et al.* Titanium carbide derived nanoporous carbon for energy-related applications. *Carbon* **44,** 2489–2497 (2006).
17. Futaba, D. N. *et al.* Shape-engineerable and highly densely packed single-walled carbon nanotubes and their application as super-capacitor electrodes. *Nature Mater.* **5,** 987–994 (2006).
18. Li, X. *et al.* Transfer of large-area graphene films for high-performance transparent conductive electrodes. *Nano Lett.* **9,** 4359–4363 (2009).
19. Bushueva, E. G. *et al.* Double layer supercapacitor properties of onion-like carbon materials. *Phys. Status Solidi B* **245,** 2296–2299 (2008).
20. Park, S., Lian, K. & Gogotsi, Y. Pseudocapacitive behaviour of carbon nanoparticles modified by phosphomolybdic acid. *J. Electrochem. Soc.* **156,** 921–926 (2009).
21. Plonska-Brzezinska, M. E., Palkar, A., Winkler, K. & Echegoyen, L. Electrochemical properties of small carbon nano-onions films. *Electrochem. Solid State Lett.* **13,** 35–38 (2010).
22. Ugarte, D. Curling and closure of graphitic networks under electron-beam irradiation. *Nature* **359,** 707–709 (1992).
23. Kuznetsov, V. L. *et al.* Effect of explosion conditions on the structure of detonation soots: ultradisperse diamond and onion carbon. *Carbon* **32,** 873–882 (1994).
24. Portet, C., Yushin, G. & Gogotsi, Y. Electrochemical performance of carbon onions, nanodiamonds, carbon black and multiwalled nanotubes in electrical double layer capacitors. *Carbon* **45,** 2511–2518 (2007).
25. Du, C. & Pan, N. High power density supercapacitor electrodes of carbon nanotube films by electrophoretic deposition. *Nanotechnology* **17,** 5314–5318 (2006).
26. Portet, C., Chmiola, J., Gogotsi, Y., Park, S. & Lian, K. Electrochemical characterizations of carbon nanomaterials by the cavity microelectrode technique. *Electrochim. Acta* **53,** 7675–7680 (2008).
27. Lin, R. *et al.* Microelectrode study of pore size, ion size and solvent effects on the charge/discharge behaviour of microporous carbons for electrical double-layer capacitors. *J. Electrochem. Soc.* **156,** 7–12 (2009).
28. Lin, R. *et al.* Solvent effect on the ion adsorption from ionic liquid electrolyte into sub-nanometer carbon pores. *Electrochim. Acta* **54,** 7025–7032 (2009).
29. Kaempgen, M., Chan, C. K., Ma, J., Cui, Y. & Gruner, G. Printable thin film supercapacitors using single-walled carbon nanotubes. *Nano. Lett.* **9,** 1872–1876 (2009).
30. Taberna, P.-L., Simon, P. & Fauvarque, J. F. Electrochemical characteristics and impedance spectroscopy studies of carbon–carbon supercapacitors. *J. Electrochem. Soc.* **150,** 292–300 (2003).
31. Huang, J. *et al.* Curvature effects in carbon nano-materials: exohedral versus endohedral supercapacitors. *J. Mater. Res.* doi: 10.1557/JMR.2010.195 (2010).
32. Banerjee, J., Perez, I., Henn-Lecordier, L., Lee, S. B. & Rubloff, G. W. Nanotubular metal–insulator–metal capacitor arrays for energy storage. *Nature Nanotech.* **4,** 292–296 (2009).

Author contributions

M.B. and D.P. conceived and designed the experiments for the elaboration of the electrochemical microcapacitors. H.D. was involved in the conception of the microdevice patterns. D.P. established the EPD process. Y.G. was involved in material synthesis and characterization. V.M. carried out the simulation of OLC formation. D.P., P.H., P.L.T. and P.S. performed the electrochemical characterizations. D.P., M.B., P.S. and Y.G. co-wrote the paper, and all authors discussed the results and commented on the manuscript.

Ultrahigh-power micrometre-sized supercapacitors based on onion-like carbon

David Pech, Magali Brunet, Hugo Durou, Peihua Huang, Vadym Mochalin, Yury Gogotsi, Pierre-Louis Taberna and Patrice Simon

SUPPLEMENTARY METHODS

Onion-Like Carbon Synthesis, Modeling and Characterization

Nanodiamond (ND) soot UD50 (Nanoblox, Inc.) was synthesized by detonation of explosives in an oxygen-free environment. Its characteristics have been described elsewhere[33]. The ND particle size is around 5 nm with a specific surface area of 350 m^2 g^{-1} and negligible pore volume. UD50 is constituted of diamond cores surrounded by graphitic carbon shells where more than 50% is sp^2 carbon. ND soot was annealed under high vacuum (10^{-6} Torr) at 1800°C for 2 h (Solar Atmosphere, PA) to produce carbon onions following the procedure described in ref. [34]. We produced carbon onions by annealing nanodiamond in the temperature range from 1200 to 2000°C. Because the specific surface area, pore size and pore size distribution remained nearly the same for samples annealed at different temperatures, but the electrical conductivity of the samples increased sharply with temperature, onions prepared at 1800°C were selected for device fabrication. Raman analysis and transmission electron microscopy (TEM) studies showed particle growth and polygonization above 1800°C.

Molecular Dynamics (MD) simulation of a spherical nanodiamond cluster of 4 nm in diameter (5995 carbon atoms) has been performed in NVT ensemble. Simulations were performed for 1 ns at 1200°C (the lowest experimentally determined temperature for ND transformation to OLC) and for 0.4 ns at 1800°C (the temperature used in our experimental study) with time steps of 0.5 fs (at 1200°C) and 0.2 fs (at 1800°C). Shorter time step was necessary to use at higher temperature to prevent ejecting extremely hot carbon atoms from the ND cluster resulting in MD run error. Brenner reactive empirical bond order REBO potential has been used[35]. The system has been allowed to reach equilibrium geometry at 300 K for 1 ps and after that the temperature was raised as desired. The atom positions were recorded every 1000 (in the case of 1200°C run) or 2000 (in the case of 1800°C run) time steps to trace the evolution of the system. The modelling was performed using GULP 3.4 module in Accelrys Materials Studio 4.4 suite. Formation of carbon onions with some imperfections was observed at both temperatures, but the ordering increased with the temperature.

Elaboration and Electrochemical Characterization of the Micro-devices

The micro-devices were elaborated as follows. Silicon dioxide (300 nm) was first thermally grown on silicon wafer followed by the evaporation of 100 nm of titanium and 800 nm of gold. The current collectors with various geometries (4, 8 and 16 interdigital fingers) on which the active material is deposited were formed by conventional photolithography and etching of the titanium/gold layer. Active materials (OLC and AC) were then deposited by electrophoretic deposition (EPD) onto the patterned current collectors, by using 0.3 wt.% of carbon in a 95 % - 5 % ethanol-water solution. In order to stabilize the carbon particles (zeta potential +12.2 ± 1.1 mV for OLC) and obtain an adherent layer, 0.03 wt.% of MgCl$_2$ were added to the suspension. It has been indeed reported that hydroxyl ions accumulated near the electrode react with Mg^{2+} ions adsorbed on the carbon particles to form magnesium hydroxide

$Mg(OH)_2$ which acts as an inorganic binder for the deposited particles[36-39]. The particle sizes (agglomerates in solution) were 0.8 ± 0.9 and 4.2 ± 1.1 μm, for the OLC and AC, respectively. A DC voltage of 50 V cm^{-1} was then applied between the micro-devices and a gold electrode. Thickness of the deposited layer was determined using SEM and confocal microscopy. The deposition rate was estimated to be around 0.5 μm min^{-1}, and the density of both OLC and AC deposit was ~0.5 g cm^{-3}.

The micro-devices were then filled with a 1M Et_4NBF_4/anhydrous propylene carbonate electrolyte in a glove box under Ar 6.0 atmosphere with H_2O and O_2 levels less than 1 ppm (in order to prevent any early oxidation of the electrolyte). They were placed in sealed cells then removed from the glove box to be connected to a Biologic VMP potentiostat to perform the electrochemical characterizations in the 2-electrode cell mode. Electrochemical impedance spectroscopy (EIS) measurements were carried out at open circuit voltage (OCV) by applying a sinusoidal signal of 10 mV amplitude at frequencies ranging from 100 kHz to 10 mHz.

Specific capacitance calculation

The cell capacitance (in F cm^{-2}) was calculated using the voltammetric discharge integrated from the cyclic voltammogram over the whole potential range (3 V) according to the following equation:

$$C = \frac{Q}{\Delta E \times S} \tag{1}$$

where Q is the charge (in C or A.s), ΔE is the potential window (in V), and S is the total surface of the positive and negative conducting electrodes (in cm^2).

The stack capacitance (in F cm^{-3}) was calculated by taking into account only the active material, the current collectors and the separator and, for all the devices tested, did not include the packaging. In the case of the micro-device, the same procedure has been used: the stack is defined from the whole projected surface area S_p (25 mm^2) including the gap between the electrodes, and taking into account the thicknesses of the current collector and the active material.

The electrochemical performance of all devices reported in the Ragone plot (Figure 4) was based on the volume of the stack and measured under the same dynamic conditions from cyclic voltammetry (using the same potential scan rate in charge and discharge) according to the following conditions.

For a given scan rate v (V s^{-1}), the discharged power P (W) was calculated by integrating the current (I) *vs.* potential (E) plots (equation (2)):

$$P = \int_0^3 I \times E \; dE \tag{2}$$

The discharged energy W (Wh) was obtained by using equation (3):

$$W = \frac{\Delta E}{v \times 3600} \times \int_0^3 I \times E \; dE \tag{3}$$

where ΔE is the discharge potential range (3V).

SUPPLEMENTARY TABLES

Average pore size (nm)	6
Specific surface area ($m^2\ g^{-1}$)	520
Raman I_D/I_G ratio	1.2
Electrical conductivity at 298 K ($S\ cm^{-1}$)	4 (powder) 2.5-3.0 (electrode)

Supplementary Table S1. Selected properties of OLC produced by graphitization of nanodiamond at 1800ºC in vacuum[24].

Number of interdigital electrodes	4	8	16
Width, w (µm)	1175.0	537.5	218.8
Length, l (mm)	4.5	4.5	4.5
Interspace, i (µm)	100	100	100
Total surface S of the conducting electrodes (mm^2)	21.15	19.35	15.75
Mean path (µm)	176.1	86.3	46.1
Total surface S_p of the cell (mm^2)	25	25	25
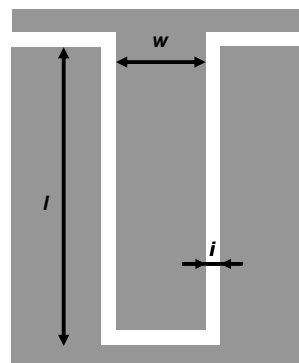
Supplementary Table S2. In order to apprehend the possible role of the micro-scale device on the electrochemical properties and particularly on the power, different configurations were designed for the elaboration and testing of electrochemical micro-capacitors. The table shows the dimensions of the micro-supercapacitors designed with 4, 8 and 16 interdigital electrodes. The mean ionic path between 2 opposite electrodes has been deduced from the geometric distance between the interdigital fingers using a Matlab[TM] routine.

SUPPLEMENTARY FIGURES
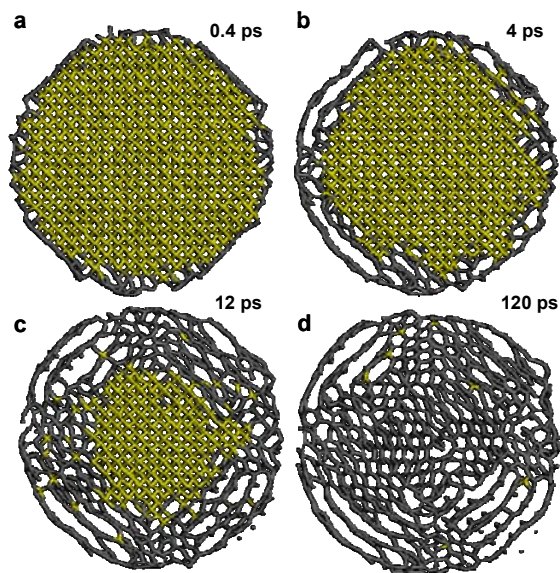
Supplementary Figure S1. Onion-like carbon. **a-d,** Molecular dynamics simulation of evolution of diamond into OLC for a nanodiamond crystal of 4 nm in diameter. 0.6 nm thick slices through the center of the particle are shown for four different times starting from the initial stage (diamond) to the fully formed graphitic onion.
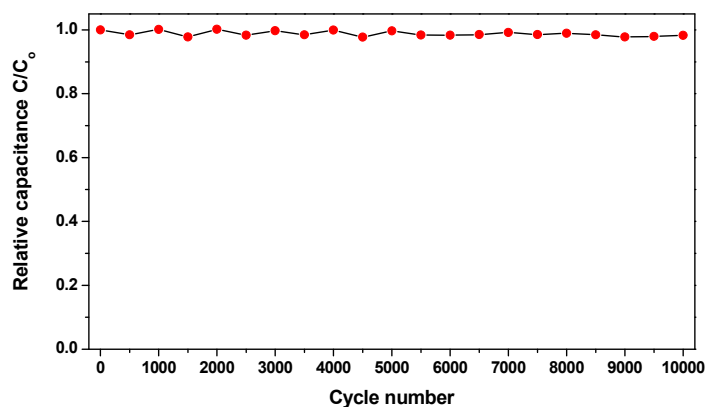
Supplementary Figure S2. Evolution of the relative capacitance *vs.* the number of electrochemical cycles at 10 $V.s^{-1}$ of a carbon onions based micro-supercapacitor made of 16 interdigital electrodes in a 1M Et_4NBF_4/ anhydrous propylene carbonate. C_o refers to the capacitance obtained for the first cycle. The capacitance remains almost unchanged after 10,000 cycles, confirming the stability of the deposited layers.
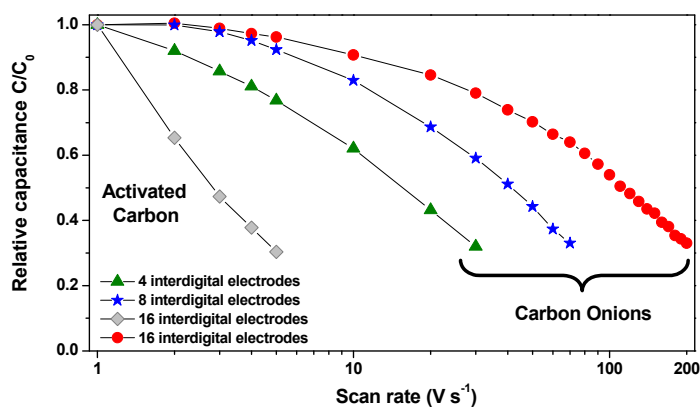
Supplementary Figure S3. Evolution of the relative capacitance *vs.* scan rate for micro-devices made of 4, 8 and 16 interdigital electrodes. The larger number of interdigital electrodes, the more power is extracted from the micro-device, stressing the key role of the device architecture in the observed breakthrough electrochemical performance. The electrolyte resistance decreases with the reduction of the mean ionic diffusion path between the electrodes, with no more ion transport limitations. A 5 μm thick layer of activated carbon in a micro-device made of 16 interdigital electrodes shows nevertheless a lower performance. It clearly demonstrates that the power ability is attributable to the combination of the carbon nanomaterial with the micro-device architecture.
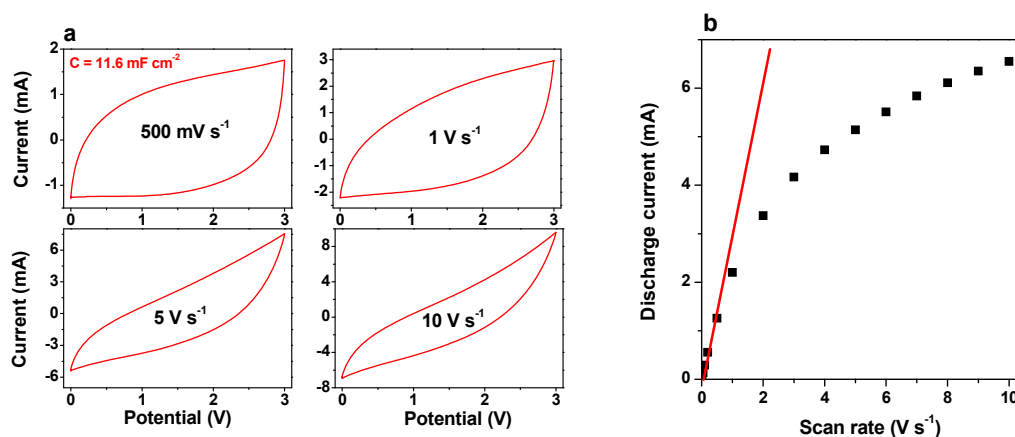
Supplementary Figure S4. a, Cyclic voltammograms obtained at different scan rates from a 16 interdigital micro-supercapacitor based on a 5 μm thick activated carbon in a 1M Et_4NBF_4/ anhydrous propylene carbonate. **b,** Evolution of the discharge current *vs.* scan rate. A linear dependence is obtained to only 1 V s^{-1}, indicating the important role of the active material.
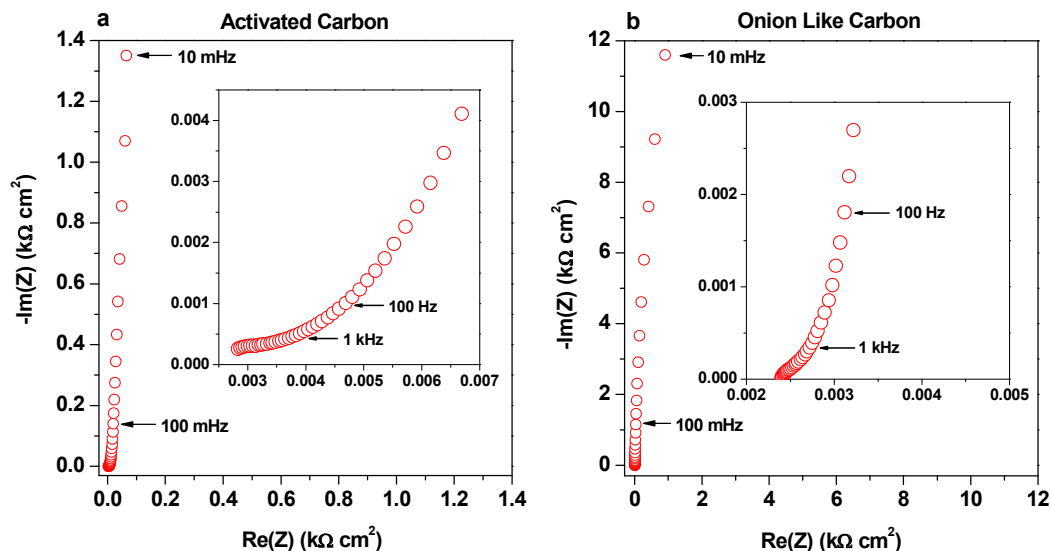
Supplementary Figure S5. Nyquist plots obtained from a 16 interdigital micro-supercapacitor in a 1M Et_4NBF_4/ anhydrous propylene carbonate. **a,** Micro-device based on activated carbon. **b,** Micro-device based on onion-like carbon. Differently from the activated carbon-based micro-device, the micro-supercapacitor containing OLC as active material shows a pure capacitive behaviour even at high frequencies (>100 Hz) thanks to the full accessible surface area offered by the carbon onions (S5b).

SUPPLEMENTARY NOTES

Supplementary References

33. Osswald, S., Yushin, G., Mochalin, V., Kucheyev, S.O. & Gogotsi, Y. Control of sp^2/sp^3 carbon ratio and surface chemistry of nanodiamond powders by selective oxidation in air. *J. Am. Chem. Soc.* **128**, 11635-11642 (2006).

34. Kuznetsov, V.L., Chuvilin, A.L., Butenko, Y.V., Mal'kov, I.Y. & Titov, V.M. Onion-like carbon from ultra-disperse diamond. *Chem. Phys. Lett.* **222**, 343-348 (1994).

35. Brenner, D.W. *et al.* A second-generation reactive empirical bond order (REBO) potential energy expression for hydrocarbons. *J. Phys. Condens. Matter.* **14**, 783-802 (2002).

36. Russ, B.E. & Talbot, J.B. An analysis of the binder formation in electrophoretic deposition. *J. Electrochem. Soc.* **145**, 1253-1257 (1998).

37. De Beer, E., Duval, J. & Meulenkamp, E.A. Electrophoretic deposition : a quantitative model for particle deposition and binder formation from alcohol-based suspensions. *J. Colloid Interface Sci.* **222**, 117-124 (2000).

38. Du C. & Pan N. Supercapacitors using carbon nanotubes films by electrophoretic deposition. *J. Power Sources* **160**, 1487-1494 (2006).

39. Besra, L. & Liu, M. A review on fundamentals and applications of electrophoretic deposition (EPD). *Prog. Mater. Sci.* **52**, 1-61 (2007).